Instability of Elliptic Jets

Philip J. Morris*
Pennsylvania State University, University Park, Pennsylvania

This paper presents a detailed account of the hydrodynamic stability characteristics of the initial region of an elliptic jet. A realistic mean velocity profile is used. Calculations of growth rates, phase velocities, and eigenfunctions are presented. The growth rates of all modes in the initial mixing region are found to depend on the minimum momentum thickness. Pressure fluctuations are found to be greatest for all modes close to the major axis. An irregular normal mode is found at larger eccentricities. All modes, odd or even about the major axis and with periods of π or 2π, have similar growth rates in the initial mixing region.

Introduction

THIS paper presents a detailed account of the hydrodynamic stability characteristics of an elliptic jet in the initial mixing region. The results of the analysis serve two purposes: 1) they provide a reference case for the verification of analyses that consider jets of arbitrary shape and 2) they provide some insight into the initial development of large-scale coherent structures in a turbulent, elliptic jet. In a previous paper,[1] the author presented some preliminary calculations. The present paper extends those calculations and corrects some misinterpretations.

Purely round jet geometries are the exception rather than the rule in practical applications. Jet engine exhausts are fitted with mixing devices to reduce noise and decrease the length of the exhaust plume. Noncircular exhausts also occur in V/STOL applications in enhanced lift and thrust-vectoring devices. The enhanced mixing properties of noncircular jets make them attractive components for fuel injection and high-speed combustion. A number of recent experimental investigations have been conducted to examine the properties of noncircular jets.[2-8] At low Reynolds numbers, an elliptic jet develops in an unusual fashion as the major and minor axes of the jet switch several times with downstream distance. This may be associated with the mutual interaction of adjacent elliptic toroidal vortices. At high Reynolds numbers, the number and location of any axis-switching remains unclear. However, in this case, experience has shown that the gross properties of the large-scale structures in the turbulent mixing layer may be modeled as instability waves. This approach has led to a better understanding of jet mixing noise radiation in high-speed jets[9] and the effect of acoustic excitation on the development of turbulent jets.[10] Detailed comparisons between the predictions of instability-wave models and turbulence in mixing layers[11] and wakes[12] have also been made. Thus, a knowledge of the stability characteristics of an elliptic jet should provide a description of the gross features of the large-scale structures in such a flow.

Crighton[13] examined the stability of an elliptic jet with a "top-hat" velocity profile. He obtained some solutions for large eccentricity, in which limit the jet had stability characteristics similar to those of a two-dimensional jet. Calculations for a wide range of eccentricities for this vortex sheet representation were obtained by Morris and Miller.[1] Their numerical results supported Crighton's asymptotic solutions. However, the vortex sheet approximation is valid only in the low-wave-number limit. It indicates instability at all frequencies. The observed limited bandwidth of unstable frequencies is determined by the finite width of the mixing region. Only by using realistic mean velocity profiles can a most unstable or neutral frequency be obtained. Thus, in the present paper, the stability of an elliptic jet represented by a continuous axial velocity profile will be considered.

A numerical method for the calculation of the stability characteristics of jets of arbitrary shape has been developed by Koshigoe and Tubis.[14] Their calculations for an elliptic jet compared favorably with the earlier calculations of Ref. 1. The integral approach that they use suffers from limitations in accuracy as will be shown below. However, the technique does not depend on the separability of the stability equations and is thus a very attractive approach.

In this paper, the stability characteristics of elliptic jets are documented for several eccentricities. The numerical solution requires the evaluation of modified Mathieu functions for arbitrary complex argument. Both eigenvalues and eigenfunctions are presented. In the next section, the stability equation in elliptic cylindrical coordinates and the asymptotic forms of solution that satisfy the boundary conditions are developed. The numerical evaluation of those asymptotic solutions is then described. The stability characteristics of an elliptic jet in the initial region are then given. Finally, the relationship between these calculations and the development of a realistic elliptic jet is discussed.

Analysis

A jet flow is considered issuing from an elliptic nozzle. The problem will be developed in elliptic cylindrical coordinates (ρ,θ,z). These are related to the Cartesian system by

$$x = a\cosh\rho\cos\theta$$

$$y = a\sinh\rho\sin\theta$$

$$z = z \tag{1}$$

The jet axis is aligned with the z direction and the axial mean velocity of the jet $W(\rho,\theta)$ is assumed to be a function of ρ and θ only. This is the parallel flow approximation of hydrodynamic stability. This assumption leads to the leading-order problem in a multiple-scales analysis to include the effects of flow divergence. These effects are not considered in the present analysis.

A Poisson equation for the pressure is obtained by taking the divergence of the momentum equation and using the equation of continuity. The resulting equation is linearized about the mean flow. The velocity fluctuations are eliminated in favor of the pressure fluctuation using the linearized momentum equations. If the pressure fluctuation is written in the form

$$p(\rho,\theta,z,t) = \hat{p}(\rho,\theta)\exp[i(\alpha z - \omega t)] \tag{2}$$

Presented as Paper 86-1868 at the AIAA 10th Aeroacoustics Conference, Seattle, WA, July 9-11, 1986; received July 14, 1986; revision received July 1, 1987.

*Professor, Department of Aerospace Engineering. Member AIAA.

then the equation for $\hat{p}$ may be written as

$$\frac{\partial^2\hat{p}}{\partial\rho^2}+\frac{\partial^2\hat{p}}{\partial\theta^2}+\frac{2\alpha}{\Omega}\left(\frac{\partial W}{\partial\rho}\frac{\partial\hat{p}}{\partial\rho}+\frac{\partial W}{\partial\theta}\frac{\partial\hat{p}}{\partial\theta}\right)-\frac{\alpha^2a^2}{2}\times[\cosh(2\rho)-\cos(2\theta)]\hat{p}=0 \tag{3}$$

where $\Omega=\omega-\alpha W$.

Only if W is taken to be a function of the "radial" coordinate ρ can a separable form of solution be sought. This separation is valuable in that highly accurate stability calculations may be performed without excessive computation. However, as will be seen below, this results in a link between the momentum thickness distribution of the mean flow and the eccentricity of the jet that may not be physically realistic.

If a solution for $\hat{p}$ is sought in the form $\hat{p}=R(\rho)T(\theta)$, then T and R are found to satisfy

$$\frac{d^2T}{d\theta^2}+[\lambda-2q\cos(2\theta)]T=0 \tag{4}$$

and

$$\frac{d^2R}{d\rho^2}+\frac{2\alpha}{\Omega}\frac{dW}{d\rho}\frac{dR}{d\rho}-[\lambda-2q\cosh(2\rho)]R=0 \tag{5}$$

where $q=-\alpha^2a^2/4$ and λ is a separation constant. In general, q is complex. Equation (4) is Mathieu's equation. Equation (5) is the Rayleigh equation in elliptic cylindrical coordinates and reduces to the modified Mathieu equation in regions where W is constant.

The solutions of Eq. (4) are of four types that are odd or even in θ and with period π or 2π. Details of the evaluation of the Mathieu and modified Mathieu functions and their characteristic numbers are given in Refs. 15 and 16. The notation given by Abramowitz and Stegan[16] is used in the present analysis. The characteristic numbers were obtained numerically as the eigenvalues of the matrix for the coefficients of the sine or cosine series of the Mathieu functions (see Ref. 16, Eqs. 20.2.2-20.2.11). The series was truncated after 11 terms. This gave eight decimal places of accuracy for all the values that could be compared with tabulated values.[16] The modified Mathieu functions were obtained from a series of products of Bessel functions (see Ref. 16, Eqs. 20.6.7-20.6.10).

Only certain combinations of these functions permit the physical boundary conditions to be satisfied. These were determined by Crighton.[13] In the ambient fluid surrounding the jet, the pressure fluctuation must vanish as $\rho\to\infty$. This leads to the following forms of solution:

$$\hat{p}(\rho,\theta)\to A\ \mathrm{ce}_{2r+p}(\theta)\mathrm{Mc}^{(3)}_{2r+p}(\rho)\to A\ \mathrm{se}_{2r+p}(\theta)\mathrm{Ms}^{(3)}_{2r+p}(\rho) \tag{6}$$

$\mathrm{Mc}^{(3)}$ and $\mathrm{Ms}^{(3)}$ are Mathieu-Hankel functions. If $p=0$, the solutions are of period π; if $p=1$, the solutions are of period 2π.

The interfocal line $\rho=0$ extends from $(x,y)=(-a,0)$ to $(a,0)$. If the pressure and velocity components are to be continuous across the interfocal line, then the solution for $\hat{p}(\rho,\theta)$ for small ρ must take the form,

$$\hat{p}(\rho,\theta)=B\ \mathrm{ce}_{2r+p}(\theta)\mathrm{ce}_{2r+p}(\rho)=B\ \mathrm{se}_{2r+p}(\theta)\mathrm{se}_{2r+p}(\rho) \tag{7}$$

This gives the asymptotic form of the solution within the potential core of the jet.

Crighton[13] considered the case of a vortex sheet representation of the jet flow, that is,

$$W(\rho)=W_0 \text{ for } \rho<\rho_0 \qquad =0 \text{ for } \rho>\rho_0 \tag{8}$$

Continuity of pressure and particle displacement at the vortex sheet requires that

$$\Delta[\hat{p}]=0;\ \Delta\left[\frac{\partial\hat{p}}{\partial\rho}\right]=0 \tag{9}$$

where $\Delta[\ ]$ denotes the change across the discontinuity. Application of these conditions for the forms of solution given by Eqs. (6) and (7) leads to a set of dispersion relationships. For the even modes these take the form,

$$\frac{\mathrm{Ce}'_{2r+p}(\rho_0)\mathrm{Mc}^{(3)}_{2r+p}(\rho_0)}{\mathrm{Ce}_{2r+p}(\rho_0)\mathrm{Mc}^{(3)\prime}_{2r+p}(\rho_0)}=\left[1-\frac{\alpha W_0}{\omega}\right]^2 \tag{10}$$

where the primes denote differentiation with respect to ρ. A similar result may be obtained for the odd solutions. Crighton[13] obtained asymptotic solutions for these relationships for large eccentricities. Morris and Miller[1] solved Eq. (10) numerically for a wide range of eccentricities. They showed that, as the eccentricity increased, the growth rates of the even modes decreased, but those of the odd modes, in particular $2r+p=1$, increased. This could be interpreted to mean that as the jet's eccentricity increases the preferred mode would switch from being in phase around the jet, such as the axisymmetric mode in the round jet, to being out of phase about the major axis, such as the antisymmetric mode in the two-dimensional jet. However, these conclusions should be valid only at very low frequencies in a real jet. These deficiencies are addressed below where a mean velocity profile with finite thickness is considered.

Calculations

Mean Velocity Profile

The mean velocity profile considered is analogous to that chosen by Michalke[17] to describe the initial mixing region of a circular jet. For the elliptic jet, the profile is taken to be

$$W(\rho)=1 \text{ for } 0\le\rho\le\rho_i \qquad =\tfrac{1}{2}\left\{1+\tanh\left[B\left(\frac{1-\sinh\rho/\sinh\rho_0}{2\theta_B}\right)\right]\right\} \text{ for } \rho>\rho_i \tag{11}$$

where A and B are the lengths of the semi-major and semi-minor axes of the ellipse defined by $\rho=\rho_0$ and θ_B is the momentum thickness along the minor axis given by

$$\theta_B=\int_0^\infty W(1-W)dy,\ x=0 \tag{12}$$

In Eq. (12), ρ_i is chosen such that $\tanh[B(1-\sinh\rho_i/\sinh\rho_0)/2\theta_B]$ is close to unity and ρ_0 is the half-velocity point. Since the minimum value of ρ is zero, this condition can be met if θ_B/B is sufficiently small. The velocity profile given by Eq. (11) reduces to Michalke's[17] profile in the case of a circular jet. The profile was chosen by Michalke on the basis of comparison with experimental data rather than being a solution of the equations of motion. As such it is a local representation,

consistent with the parallel flow approximation of the stability analysis. Axial variations are included parametrically through the dependence of θ_B and B on z. The validity of this choice of profile may be seen by comparing with the experimental data of Ho and Gutmark.[8] Figure 1 shows a comparison made at two axial locations $z/A_0 = 0.5$ and 2.0, where A_0 is the semi-major axis length at the jet exit. The local values of A/B based on the locations of the half-velocity points are 1.88 and 1.49, respectively. The corresponding values of θ_B/B were found to be 0.044 and 0.223. The agreement between the analytical profile and experimental data is reasonably good, except in the inner part of the mixing region along the minor axis for the downstream location.

The momentum thickness along the major axis is defined by

$$\theta_A = \int_0^\infty W(1-W)\mathrm{d}x, \quad y=0 \tag{13}$$

It can be shown that

$$A\theta_A = B\theta_B[1 + \text{ terms of order}(\theta_B/B)^2] \tag{14}$$

Thus, as the eccentricity of the jet increases the momentum thickness on the minor axis becomes greater than that on the major axis. This is a consequence of requiring that W be a function of ρ only so that a separable solution can be obtained. In practice, this linkage between eccentricity and momentum thickness ratio will not exist. In that sense, the profile is somewhat unrealistic. However, the benefits of obtaining highly accurate solutions to the separable problem are felt to justify the present approach.

Numerical Method

The Rayleigh equation (5) was solved numerically using a variable step-size Runge-Kutta algorithm (IMSL routine DVERK modified for complex arithmetic). For a given value of frequency and initial guess for the wavenumber, two integrations were performed starting from ρ_1 and ρ_2, at which $W = 0.001$ and 0.999, respectively, toward the center of the mixing region. The starting conditions were based on the asymptotic solutions [Eqs. (6) and (7)]. The resulting numerical solutions at $\rho = \rho_0$ are denoted by $R_1(\rho_0)$ and $R_2(\rho_0)$. The two solutions and their derivatives much match at $\rho = \rho_0$, that is,

$$C_1R_1(\rho_0) - C_2R_2(\rho_0) = 0$$

$$C_1R_1'(\rho_0) - C_2R_2'(\rho_0) = 0 \tag{15}$$

If Eq. (15) is to have a nontrivial solution for C_1 and C_2,

$$\nabla(\omega,\alpha) = R_1(\rho_0)R_2'(\rho_0) - R_1'(\rho_0)R_2(\rho_0) = 0 \tag{16}$$

Newton's method was used to find the zeroes of $\nabla(\omega,\alpha)$ and hence the eigenvalues α.

Calculations were performed for both odd and even modes about the major axis with periods π and 2π. The variables were nondimensionalized with respect to jet exit velocity, radius of a circular jet of equal exit area $\sqrt{AB}$, and uniform density. Unless stated otherwise, all calculations were for a momentum thickness on the major axis of $\theta_A = 0.02$. However, it should be remembered that the momentum thickness on the minor axis varies according to Eq. (14). Calculations have been performed for three eccentricities: $A/B = 1.001$, 2.0, and 4.0. The first case permits comparison of the results with the circular jet case. The areas within the contours of $\rho = \rho_0$, which are the contours of the half-velocity points, were held constant.

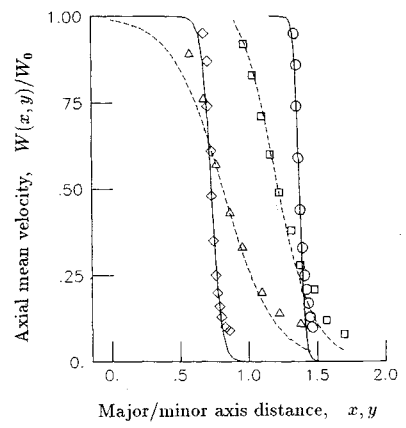

Fig. 1 Comparison of Eq. (11) with experimental data.[8] At $z/A_0 = 0.5$: ○ major axis, ◇ minor axis; at $z/A_0 = 2.0$: □ major axis, △ minor axis (from Eq. (11), —— $A/B = 1.88$, $\theta_B/B = 0.044$; ----- $A/B = 1.49$, $\theta_B/B = 0.223$).

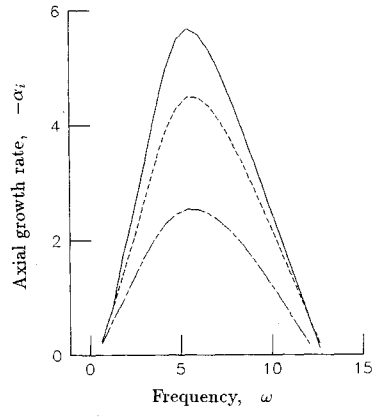

Fig. 2 Variation of axial growth rate with frequency for the ce_0 mode for $\theta_A = 0.02$ (—— $A/B = 1.001$; ----- $A/B = 2.0$; ——— $A/B = 4.0$).

Table 1 Frequencies and wave numbers for maximum rate of growth

Mode	A/B	ω_{max}	α_{real}	α_{imag}
ce_0	1.001	5.4413	10.1992	$-5.6852i$
ce_0	2.0	5.6578	10.1355	$-4.5074i$
ce_0	4.0	5.6518	9.0558	$-2.5470i$
ce_2	1.001	5.4949	10.3593	$-5.5483i$
ce_2	2.0	4.4171	8.3818	$-3.1567i$
ce_4	1.001	5.6203	10.7420	$-5.1763i$
se_1	1.001	5.4537	10.2381	$-5.6491i$
se_1	2.0	5.0106	9.3223	$-3.6778i$
se_1	4.0	3.5184	6.7366	$-2.2132i$
se_3	2.0	3.9380	7.5734	$-2.7856i$
ce_1	1.001	5.4567	10.2432	$-5.6517i$
ce_1	2.0	5.6577	10.0272	$-4.5074i$
ce_1	4.0	5.6517	9.0556	$-2.5470i$

ce_0 Mode

The ce_0 mode corresponds to the axisymmetric $m = 0$ mode in the circular jet case. Figure 2 shows the axial growth rates α_i for the ce_0 mode as the eccentricity changes. The results for $A/B = 1.001$ are very close to the circular jet results.[18] The maximum growth rate decreases as A/B increases. However, the frequency for the maximum growth remains nearly independent of eccentricity. Table 1 gives this frequency and the corresponding wave number for several modes and values of A/B. If the frequencies for maximum growth are nondimensionalized with respect to the major

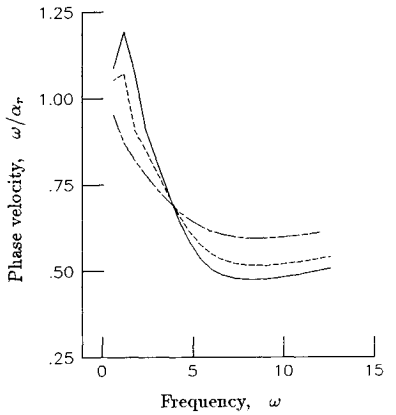

Fig. 3 Variation of phase velocity with frequency for the ce_0 mode (see Fig. 2 for legend).

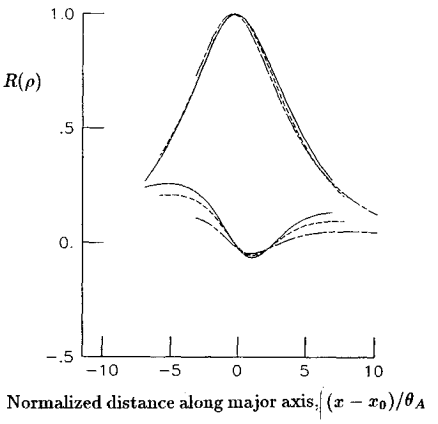

Fig. 5 Distributions of most unstable ce_0 eigenmodes along the major axis (see Fig. 2 for legend).

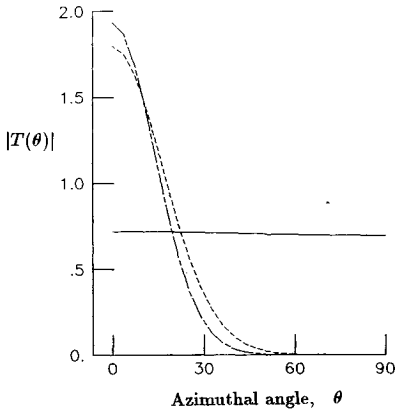

Fig. 4 Azimuthal variation of the amplitudes of the most unstable ce_0 eigenmodes (see Fig. 2 for legend).

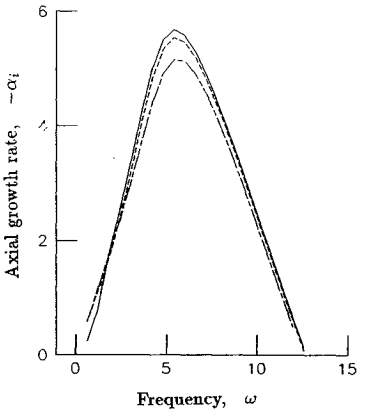

Fig. 6 Variation of axial growth rate with frequency for the ce_{2r} modes for $A/B = 1.001$, $\theta_A = 0.02$ (—$r=0$, ----- $r=1$, ——— $r=2$).

axis momentum thickness θ_A, the values for $\omega_{max}\theta_A$ are 0.109, 0.113, and 0.113 for $A/B = 1.001$, 2.0, and 4.0, respectively. This suggests that the initial shedding frequency is controlled by the minimum momentum thickness, along the major axis in the present case, and is nearly independent of eccentricity. This is confirmed by the measurements of Husain and Hussain[2] and Gutmark et al.[3,4] In the former experiments, the momentum thickness was nearly independent of azimuthal position, whereas in the latter experiments $\theta_B = 0.8\theta_A$.

Figure 3 shows the variation of the phase velocity with A/B for the ce_0 mode. For $A/B = 1.001$ the mode exhibits phase velocities greater than the exit velocity that was discussed by Bechert and Pfizenmaier.[19] In general, increasing the eccentricity makes the phase velocities less dependent on frequency. Table 1 shows that the phase velocity for ω_{max} increases with increasing A/B.

In the round jet, the amplitude of the azimuthal modes are independent of the azimuthal location. However, the behavior of modes for the elliptic jet is different. First, as discussed further below, the modes are not "spinning" but have a fixed phase reference to the major or minor axes. Second, the azimuthal variation is determined by the behavior of the Mathieu function that is the solution of Eq. (4). As A/B approaches unity, q approaches zero since a goes to zero. Then, the solutions to Eq. (4) are either sines or cosines. However, for larger values of A/B, q is a complex number with phase determined by the complex wave number α. In this case, the amplitude of the ce_0 mode is no longer independent of azimuthal location. Figure 4 shows the azimuthal variation of $|T(\theta)|$ for the various eccentricities for the maximum amplifying frequency in each case. For $A/B = 1.001$, the amplitude is nearly independent of θ. This is the axisymmetric mode behavior for the round jet. For $A/B = 2.0$ and 4.0, the amplitude decays rapidly away from the major axis and is essentially zero on the minor axis. This would indicate that close to the jet exit the pressure and velocity fluctuations associated with the ce_0 mode would be greatest near to the major axis. However, because of the form of velocity profile chosen, this is also the location of the minimum momentum thickness. For uniform momentum thickness around the jet exit, it is not clear that this behavior would be seen. The variation of $R(\rho)$ with eccentricity is shown in Fig. 5. The distribution is plotted along the major axis relative to the half-velocity point and stretched by the major axis momentum thickness θ_A. Plotted in this way, the distributions are nearly independent of eccentricity. Thus, those motions observed in the round jet will be duplicated in the elliptic jet, except that the amplitude may vary azimuthally.

ce_{2r} Modes

In addition to the ce_0 mode, there are other even modes of period π that are unstable in the initial mixing region. Figure 6 shows the axial growth rates for these ce_{2r} modes for $r = 0$, 1, and 2 for $A/B = 1.001$. From this figure and the numerical values given in Table 1, it is clear that the higher-order modes have similar but smaller growth rates than the ce_0 mode. The azimuthal variation of these modes for $A/B = 1.001$ is given approximately by $\cos(2r\theta)$. The ce_2 mode corresponds to the $n = 2$ double helix in the round jet calculations of Mattingly and Chang.[20] However, it should be emphasized that all the modes in the elliptic jet case are phase locked with respect to the major and minor axes and are not spinning modes. This means that any jet that deviates slightly from axisymmetry in the mean is likely to exhibit "flapping" rather than spinning modes.

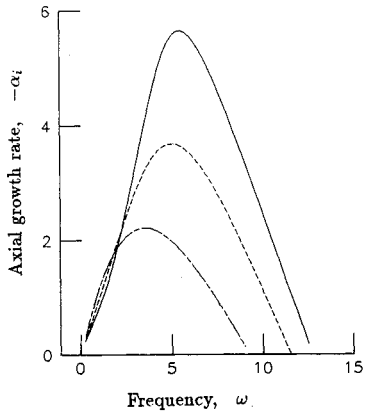

Fig. 7 Variation of axial growth rate with frequency for the se_1 mode (see Fig. 2 for legend).

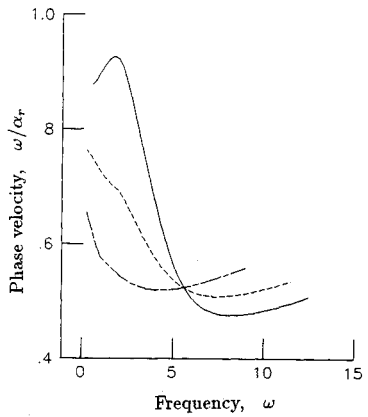

Fig. 8 Variation of phase velocity with frequency for se_1 mode (see Fig. 2 for legend).

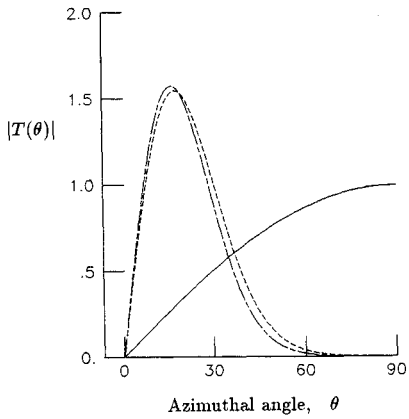

Fig. 9 Azimuthal variation of the amplitudes of the most unstable se_1 eigenmodes (see Fig. 2 for legend).

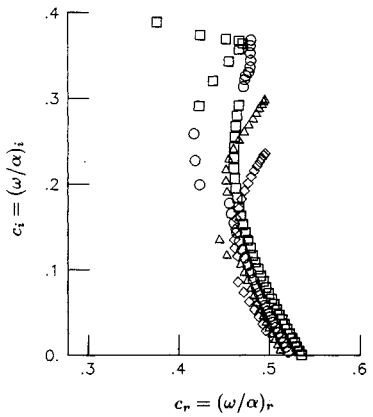

Fig. 10 Eigenvalues in the c plane for different characteristic numbers of Mathieu's equation (eigenvalue sequence number: □ 1, ○ 2, △ 3, ◇ 4).

Koshigoe and Tubis[14] have also calculated the stability of these higher-order modes. However, the accuracy of their technique, designed for nonseparable problems, is limited by their two-dimensional grid. In the present calculation, the solutions are analytic in the azimuthal direction and use a variable step size to achieve a prescribed accuracy in the "radial" direction. However, in spite of the relatively crude nature of their grid, the results in Ref. 14 show all the qualitative characteristics of the present results.

se_1 Mode

The modes that reduce to the helical, $n=1$ mode in the round jet case are the se_1 and ce_1 modes. They have azimuthal variations that reduce to $\sin\theta$ and $\cos\theta$, respectively. The variation of the axial growth rates for the se_1 mode for various eccentricities is shown in Fig. 7. For $A/B=4.0$, the maximum growth rate for the se_1 mode is slightly less than that of the ce_0 mode. The most amplifying frequencies for the se_1 mode are also slightly lower than the ce_0 modes. The value of ω_{max} falls from 0.1091 to 0.0704 (when scaled by the momentum thickness θ_A) as A/B changes from 1.001 to 4.0. The phase velocities, shown in Fig. 8, are always less than the jet exit velocity. For $A/B=1.001$, the results agree closely with the values for the $n=1$, helical mode in the round jet. At the most amplifying frequency, the phase velocities are approximately one-half the jet velocity (see Table 1). As the eccentricity increases, the phase velocities become less dependent on frequency.

For $q=0$, the round jet limit, the se_1 Mathieu function has its maximum value at $\theta=\pm\pi/2$. However, for other values of q, this changes. Figure 9 shows the azimuthal variation of $|T(\theta)|$ for various eccentricities. As was found in the ce_0 mode case, the amplitude falls to zero at the minor axis as the eccentricity increases. Thus, the pressure and velocity fluctuations associated with this mode will also be greater close to the major axis (for the present choice of mean velocity profile).

se_{2r+1} Modes

The higher-order odd modes with period 2π, the se_{2r+1} modes, exhibit an interesting behavior. For real or small q, the characteristic numbers of Mathieu's equation are readily classified. However, for complex q, pairs of these characteristic numbers are equal. The location of these branch points has been examined by Hunter and Guerrieri.[21] The asymptotic formulas used to calculate the characteristic numbers change as one crosses a branch cut that extends radially outward from the branch point in the complex plane (see Fig. 4, Ref. 21). Across these branch cuts, the characteristic numbers exchange their order. This leads to an unusual behavior for the se_{2r+1} modes for higher eccentricities. The characteristic numbers and the associated normal modes may be classified initially according to the eigenvalue sequence provided by the IMSL routine. Figure 10 shows the complex value of $c=\omega/\alpha$ for the first four characteristic numbers in the sequence. The eigenvalues fall into several groups. There are three continuous sequences associated with the second and first, third and second, and fourth and third characteristic numbers. There is clearly another sequence with a different behavior in the c plane that has contributions from all the characteristic numbers. This sequence could be thought of as indicating an "irregular" mode, although it does not have the same features as the irregular mode described by Michalke.[22] In the present case, the higher-order odd modes have been classified by number if they fall into the smooth sequences shown in Fig. 10 or as irregular if they do not. This leads to the axial growth rates and phase velocities shown in Figs. 11 and 12,

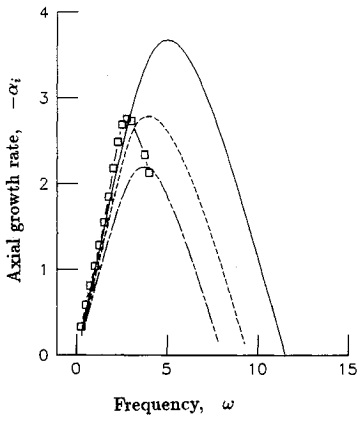

Fig. 11 Variation of axial growth rate with frequency for the se_{2r+1} modes for $A/B=2.0$, $\theta_A=0.02$ (———$r=0$, – – – –$r=1$, ——–$r=2$, □ —— □ irregular mode).

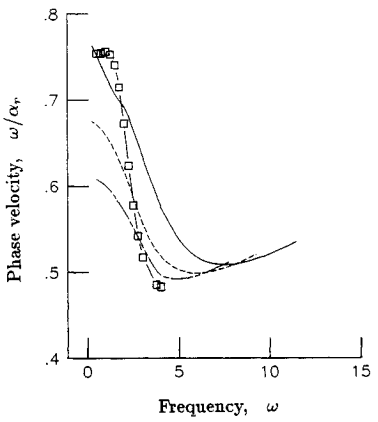

Fig. 12 Variation of phase velocity with frequency for the se_{2r+1} modes (see Fig. 11 for legend).

respectively, for $A/B=2.0$. The maximum growth rate is still associated with the se_1 mode. All the modes have similar phase velocities in the range of 0.5–0.8 and the dependence on frequency decreases as the mode number increases. Although it appears likely that the appearance of the irregular mode is associated with the branch points of the characteristic numbers of Mathieu's equation, the mode switching does not always occur near the branch cuts identified by Hunter and Guerrieri.[21] So the appearance of the irregular mode remains unexplained.

ce_{2r+1} Modes

The ce_{2r+1} modes are even about the major axis and have a period 2π. They may be identified with a flapping motion about the minor axis in the elliptic jet. The ce_1 mode corresponds to the $n=1$, helical mode in the round jet. From Table 1, it can be seen that the ce_1 and se_1 modes have almost identical characteristics, approaching the $n=1$, helical mode values as the round jet limit is approached. The ce_1 and se_1 modes behave very similarly as the eccentricity changes with the exception that the frequency of the most amplifying mode is nearly independent of the eccentricity for the ce_1 mode. In view of the similarity between the two modes, the growth rates and phase velocities are not shown, but the most amplifying frequencies and wave numbers are given in Table 1.

Discussion

The present results, subject to the particular mean velocity profile, indicate that no particular mode is dominant in the initial mixing region and that the stability characteristics are controlled by the minimum initial momentum thickness, which in the present case always lies on the major axis. In a given experiment, the selection of a particular mode will depend on external influences, such as intended or unintended forcing or a feedback based on the preferred mode of the entire jet flowfield.

Michalke[23] and others have shown how the process of vortex pairing may be simulated qualitatively using linear stability theory. Such calculations can describe the initial mixing region of a low Reynolds number jet or an artificially excited jet at higher Reynolds number. Consider the ce_0 mode corresponding to the axisymmetric mode in the round jet case. In the preceding section, it was shown that the "radial" eigenfunctions for this mode were independent of eccentricity; see Fig. 5. Thus, the same processes observed in the round jet should occur in the elliptic jet. However, in the elliptic jet, the amplitude of these motions was seen to be dependent on the azimuthal location. For the ce_0 mode, the amplitude is a maximum on the major axis and falls rapidly to zero on the minor axis. Thus, it could be speculated that a vortex roll-up would occur on the major axis, but that no such motions would be seen on the minor axis. Such vortex motions, which resulted in a switching of the jet's major and minor axes, were observed by Husain and Hussain[2] and Gutmark and Ho.[6] However, these processes occur in regions where the jet is developing rapidly and the thickness of the mixing layer is increasing.

The primary purpose of this paper has been to establish the stability characteristics of a noncircular jet. The choice of mean velocity profile enabled the stability equation to be separated so that highly accurate solutions could be obtained to the resulting ordinary differential boundary value problem. The particular choice of velocity profile resulted in an initial momentum thickness that varied around the jet, being a minimum on the major axis and a maximum on the minor axis. This situation could be different in a given experiment as it was in the measurements of Husain and Hussain[2] and Gutmark and Ho.[3] However, the results given in the preceding sections should serve as a test of the accuracy of numerical methods that describe the stability of jet flows of arbitrary shape.

Acknowledgments

This work was supported in part by NASA Langley Research Center under NASA Grant NAG-1-657. The cotechnical monitors were Drs. J.M. Seiner and R.G. Wilmoth. The author is also grateful to Prof. C.-M. Ho for supplying his experimental data and Dr. S. Koshigoe for copies of his results. The original Mathieu function routines were written by Mr. D.G. Miller.

References

[1]Morris, P.J. and Miller, D.G., "Wavelike Structures in Elliptic Jets," AIAA Paper 84-0399, 1984.

[2]Husain, H.S. and Hussain, A.K.M.F., "Controlled Excitation of Elliptic Jets," *The Physics of Fluids,* Vol. 26, Oct. 1983, pp. 2763–2766.

[3]Gutmark, E. and Ho, C.-M., "Near-Field Pressure Fluctuations of an Elliptic Jet," *AIAA Journal,* Vol. 23, 1984, pp. 354–358.

[4]Schadow, K.C., Wilson, K.J., Lee, M.J., and Gutmark, E., "Enhancement of Mixing in Ducted Rockets with Elliptic Gas-Generator Nozzles," AIAA Paper 84-1260, 1984.

[5]Gutmark, E., Schadow, K.C., Parr, D.M., Harris, C.K., and Wilson, K.J., "The Mean and Turbulent Structure of Noncircular Jets," AIAA Paper 85-0543, 1985.

[6]Gutmark, E. and Ho, C.-M., "Visualization of a Forced Elliptic Jet," *AIAA Journal,* Vol. 24, 1985, pp. 684–685.

[7]Schadow, K.C., Wilson, K.J., Parr, D.M., and Gutmark, E., "Mixing Characteristics of a Ducted Elliptical Jet with Dump," AIAA Paper 86-1399, 1986.

[8]Ho, C.-M. and Gutmark, E., "Vortex Induction and Mass Entrainment in a Small Aspect Ratio Elliptic Jet," submitted for publication.

[9]Tam, C.K.W. and Morris, P.J., "The Radiation of Sound by the Instability Waves of a Compressible Plane Turbulent Shear Layer," *Journal of Fluid Mechanics,* Vol. 98, 1980, pp. 349–381.

[10]Tam, C.K.W. and Morris, P.J., "Tone Excited Jets, Part V: A Theoretical Model and Comparison with Experiment," *Journal of Sound and Vibration,* Vol. 102, 1985, pp. 119-151.
[11]Tam, C.K.W. and Chen, K.C., "A Statistical Model of Turbulence in Two-Dimensional Mixing Layers," *Journal of Fluid Mechanics,* Vol. 92, 1979, pp. 303-326.
[12]Gaster, M., Kit, E., and Wygnanski, I., "Large-Scale Structures in a Forced Turbulent Mixing Layer," *Journal of Fluid Mechanics,* Vol. 150, 1985, pp. 23-39.
[13]Crighton, D.G., "Instability of an Elliptic Jet," *Journal of Fluid Mechanics,* Vol. 59, 1973, pp. 665-672.
[14]Koshigoe, S. and Tubis, A., "Wave Structures in Jets of Arbitrary Shape. I. Linear Inviscid Spatial Stability Analysis," *Physics of Fluids,* Vol. 29, 1986, pp. 3982-3992.
[15]McLachlan, N.W., *Theory and Application of Mathieu Functions,* Oxford University Press, London, 1947.
[16]Abramowitz, M. and Stegan, I.A., *Handbook of Mathematical Functions,* Dover, New York, 1965.
[17]Michalke, A., "Instabilitat eines kompressiblen runden Friestrahls unter Berucksichtigung des Einfluses der Strahlgrenzschichtdicke," *Zeitschrift fuer Flugwissenschaften,* Vol. 19, 1971, pp. 319-328.
[18]Morris, P.J., "The Spatial Viscous Instability of Axisymmetric Jets," *Journal of Fluid Mechanics,* Vol. 77, 1976, pp. 511-529.
[19]Bechert, D. and Pfizenmaier, E., "On Wavelike Perturbations in a Freejet Travelling Faster than the Mean Flow in the Jet," *Journal of Fluid Mechanics,* Vol. 72, 1975, pp. 341-352.
[20]Mattingly, G.E. and Chang, C.C., "Unstable Waves on an Axisymmetric Jet Column," *Journal of Fluid Mechanics,* Vol. 65, 1974, pp. 544-560.
[21]Hunter, C. and Guerrieri, B., "The Eigenvalues of Mathieu's Equation and Their Branch Points," *Studies in Applied Mathematics,* Vol. 64, 1981, pp. 113-141.
[22]Michalke, A., "Survey on Jet Instability Theory," *Progress in Aerospace Sciences,* Vol. 21, 1984, pp. 159-199.
[23]Michalke, A., "Vortex Formation in a Free Boundary Layer According to Stability Theory," *Journal of Fluid Mechanics,* Vol. 22, 1965, pp. 371-383.